RSC Advances

PAPER

View Article Online
View Journal | View Issue

Cite this: *RSC Adv.*, 2020, **10**, 33965

Properties of PEDOT nanowire/Te nanowire nanocomposites and fabrication of a flexible thermoelectric generator

Haihui Liu, * Pengfei Liu, Mengqi Zhang, Zihan Tian, Ning Wang, Yanxin Liu and Xingxiang Zhang

Received 10th March 2020
Accepted 2nd September 2020

DOI: 10.1039/d0ra02223c

rsc.li/rsc-advances

Light-weight, mechanically flexible, transparent thermoelectric devices are promising as portable, and easy-to-integrate energy sources. Poly(3,4-ethylenedioxythiophene) nanowires (PEDOT NWs) possessing high electrical conductivity were synthesized by a facile self-assembled micellar soft-template method. And then, Te nanowires (Te NWs) with high Seebeck coefficient were easily synthesized by the solution process and then added as an inorganic filler to form the PEDOT NW/Te NW nanocomposite films *via* a simple and convenient vacuum filtration method. The thermoelectric (TE) properties of the nanocomposites were characterized in this research. A maximum power factor of 58.03 μW m^{-1} K^{-2} is obtained from the film containing 90 wt% Te NWs at room temperature, which is dozens of times that of the pure PEDOT NW film. This work uses the as-prepared PEDOT NWs/Te NW (90 wt%) nanocomposite film to fabricate a flexible thermoelectric generator and an output voltage of 2.8 mV was generated at a temperature difference of 13.5 K between the environment and human body.

1. Introduction

In recent years, thermoelectric generator (TEG) devices have gradually been recognized as a viable alternative to power generating applications.[1–3] Thermoelectric generator devices can directly convert thermal energy that passes through them into electricity, which is a pollution-free, convenient and safe conversion technology, and plays an irreplaceable role in environmental friendliness and sustainable development. With the continuous development of portable/wearable and self-powered electronic devices, flexible thermoelectric generators have become a promising power source.[4,5] The advantage of thermoelectric generators is that they have no moving parts and can run continuously without any need for supplementary materials.[6] And flexible thermoelectric generators benefit wearable applications due to their good fit with human skin, thus helping to collect human heat with minimal energy loss.[7] The efficiency of a TE generator is governed by the thermoelectric materials' figure of merit ZT, $ZT = S^2\sigma/\kappa$, where T is the absolute temperature, S is the Seebeck coefficient, σ is the electrical conductivity, κ is the thermal conductivity and the power factor (PF) is $S^2\sigma$. Applied to the field of thermoelectric, materials should exhibit a large power factor and low thermal conductivity.[8] However, for a given material, the S, σ and κ of thermoelectric materials are highly interdependent and conflict with each other, which causes the difficulty in obtaining high ZT.[9,10]

Conventional inorganic materials such as Bi_2Te_3,[11] PbTe[12] and Sb_2Te_3 (ref. 13) have attracted wide attention due to their outstanding thermoelectric properties. However, the expensive raw materials, poor processability and the toxicity restrict the application of inorganic materials in the field of thermoelectrics.[14–16] Conducting polymers are now believed to be potential candidates for TE materials.[17–19] Conducting polymers possess many advantages of light-weight, low cost, mechanical flexibility and enabling the development of portable and wearable thermoelectric devices.[20–22] The development of portable/wearable TE devices has become an area of increasing interest because this device has the potential to use the temperature difference between the human body and its environment to continuously convert human body heat into electrical energy.[23] Moreover, their thermal conductivity is also much lower than that of inorganic materials, which is beneficial to the enhancement of the ZT value. Poly(3,4-ethylenedioxythiophene) (PEDOT) is one of the most promising polymer materials for practical applications in thermoelectric device due to the stability and high conductivity of the p-doped state.[24,25] In order to improve the solubility, PEDOT needs to be emulsified with PSS in water to form PEDOT:PSS. But the PEDOT:PSS film prepared from its aqueous solution has the electrical conductivity of 0.15 ± 0.01 S cm^{-1},[26] because in the mixture of PEDOT and PSS, PEDOT is responsible for conducting, whereas PSS is insulated. In general, there are two strategies to optimize the thermoelectric properties of the PEDOT:PSS. In one strategy, it can be secondly doped by a range of chemicals, including ethylene glycol (EG),[27] dimethyl sulfoxide (DMSO)[28,29] or sulfuric

Tiangong University, No. 399, West Binshui Road, Xi Qing District, Tianjin, 300387, China. E-mail: haihui_liu@aliyun.com

acid (H_2SO_4).[30–32] The excess insulating PSS could be removed by treatments process and the PEDOT component transforms from a coil to a expanded-coil or linear conformation, leading to an enhancement of electrical conductivity while the Seebeck coefficient remained essentially constant.[33] In the another strategy, PEDOT:PSS can be mixed with inorganic components which possess large Seebeck coefficients to form PEDOT:PSS/inorganic composites, such as PEDOT:PSS/Bi_2Te_3,[34] PEDOT:PSS/PbTe[35] and PEDOT:PSS/SnSe.[36] One-dimensional (1D) nanostructures of inorganic materials were typically used as filers to improve the TE properties. One-dimensional Te nanostructures are widely used as inorganic filers to mix with polymer because of the high Seebeck coefficients, the interface phonon scattering effect and the quantum size effect.[37,38] In addition to the "energy-filtering" process,[39] low-energy carriers are preferentially scattered by the potential barrier at the more interface between polymer matrix and inorganic nanostructures, whereas high-energy carriers easily through cross these barriers, resulting in an increase in *S*. See *et al.*[40] reported the hybrid materials of PEDOT:PSS/Te nanorods exhibit a large room temperature *ZT* of 0.1. Song *et al.*[41] prepared PEDOT:PSS/PF-Te composites and a maximum power factor of 51.4 $\mu W\ m^{-1}\ K^{-2}$ was obtained for the composite film containing 70 wt% PF-Te.

In this work, we have firstly prepared one-dimensional PEDOT NWs, which does not need to be mixed with PSS but have good water solubility, and then, we choose Te NWs as inorganic filler to mixed with PEDOT NWs to optimized the TE properties of materials by taking the advantages of the high *S* of the Te NWs and the low κ of the polymer. The nanocomposite film has excellent room temperature power factor. The Seebeck coefficient and electrical conductivity of the PEDOT NWs/Te NWs (90 wt%) from 100 to 300 K are also reported. The prepared thermoelectric film device shows excellent power generation capacity and the novel method for manufacturing thermoelectric device with PEDOT NWs/Te NWs (90 wt%) composite film provides a good application prospect of the polymer/inorganic flexible materials in the field of portable/wearable thermoelectric devices.

2. Experimental

2.1 Materials

3,4-Ethylenedioxythiophene (EDOT, purity > 99%), sodium dodecyl sulfate (SDS, AR), anhydrous ferric chloride ($FeCl_3$, AR), tellurium dioxide (TeO_2, 99.99%), polyvinyl pyrrolidone (PVP, MW ~ 43 000) and L-ascorbic acid (AA, 99%) were purchased from Aladdin. Potassium hydroxide (KOH, ≥85%), and ethyl alcohol (AR) were provided by Tianjin Fengchuan Chemical Reagents Factory. Ethylene glycol (EG, ≥99%) was provided by Guangfu Fine Chemical Research Institute. All chemical reagents were used as received.

2.2 Synthesis of PEDOT NWs and Te NWs

PEDOT NWs were synthesized by EDOT monomer with cylindrical SDS micellar as template. First, desired amounts of 1.08 g SDS were dissolved in distilled water to form micellar solution. Then, an aqueous solution of $FeCl_3$ (0.304 g $FeCl_3$ dissolved in 10 mL water) was injected into the above micellar solution to promote the transformation from aspherical micelles to cylindrical micellar with stirring at property temperature. Finally, EDOT monomer was slowly added into the micellar solution and the polymerization was subsequently induced by $FeCl_3$. The whole reaction was carried out at 50 °C with continuous stirring for 6 h. Finally, the obtained products were centrifuged and washed repeatedly with ethanol and deionized water.

For synthesis of Te NWs, 15 mL EG, 1.5 g KOH, 0.5 g PVP and 0.16 g TeO_2, were added into a three-neck flask. And then the mixture was heated to 120 °C under nitrogen. Meanwhile, 1.89 M L-ascorbic acid aqueous solution was prepared in a beaker by stirring and heating to 80 °C. 3 mL of 1.89 M L-ascorbic acid solution was rapidly injected as a reducing agent into the mixture solution when it reached to 120 °C. The Te NWs were successfully synthesized after the reaction process was performed at 120 °C for 24 h. The as-synthesized Te NWs were separated from solution by centrifugation at 8000 rpm for 40 min. And the Te NWs were then redissolved in 1 M potassium hydroxide aqueous to remove the residual PVP. Finally, the obtained Te NWs were centrifuged and washed several times with deionized water and ethanol.

2.3 Sample preparation

The PEDOT NWs aqueous solution was mixed with the Te NWs aqueous solution at the designed ratios. Then the mixture solution was ultrasonically dispersed for 10 min. The porous PTFE membrane (0.45 μm) as a base and the simple vacuum filtration was used to prepare PEDOT NWs/Te NWs nanocomposite thin films. Finally, the as-prepared nanocomposite films were dried at 50 °C under vacuum for 12 h.

2.4 Characterization

Transmission electron microscopy (TEM) images were observed by a Hitachi H7650 transmission electron microscope operating at 120 kV. Scanning Electron Microscope (SEM) images were obtained by a ZEISS Gemini SEM500 scanning electron microscope operating at 20 kV. The wide-angle X-ray patterns were collected by a Bruker D8 ADVANCE X-ray diffractometer with Cu $K\alpha_1$ (λ = 1.541 Å) radiation. The Seebeck coefficient of nanocomposite films was measured by a portable Seebeck coefficient tester (PTM-demo). For electrical conductivity, Hall effect testing instrument (Swin HALL8800) was used. The characterization of thermal conductivity was tested by the thin film material testing equipment produced by Beijing Multi-field Technology Company.

3. Results and discussion

The morphology of the prepared PEDOT NWs and Te NWs are characterized by TEM. Fig. 1a shows the clearly microscopic morphology of the prepared PEDOT NWs. A nanowire bundle consists of many individual nanowires. The average diameter of a single PEDOT NWs is about 100 nm and the length of

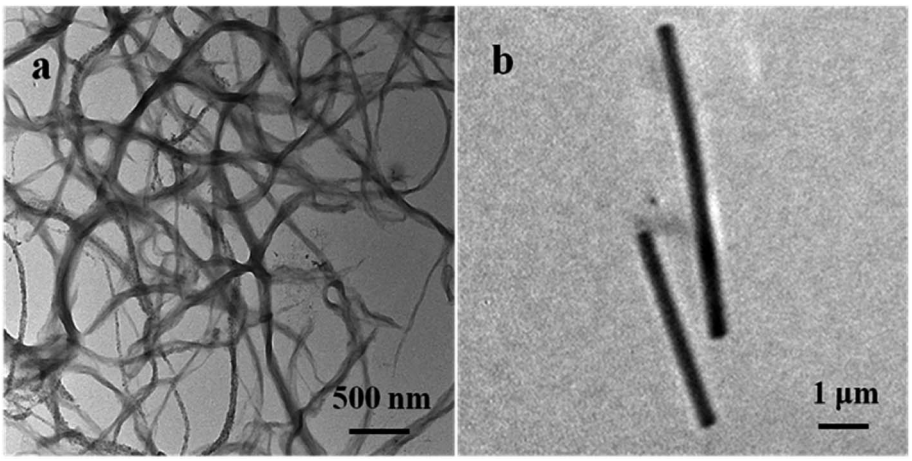

Fig. 1 TEM images of the PEDOT NWs (a) and Te NWs (b).

nanowires can reach several micrometers. As the Fig. 1b shown, it can be observed that the surface of Te NWs is relatively smooth and uniform in size with a diameter of about Te NWs 400 nm and a length of up to 10 μm.

The XRD peaks are shown in Fig. 2a, all diffraction peaks of the synthesized Te NWs are consistent with the crystal structure of pure Te phase, and it can be indexed to a trigonal structure Te phase with lattice parameters of $a = 4.4328$ Å and $c = 5.9466$ Å, which are consistent with the standard PDF card (JCPDS card no. 36-1452). No diffraction peaks of other phases were detected, indicating that we obtained the pure Te NWs by solution process. As showed in Fig. 2b, the broad peak at $2\theta = 25.8°$ corresponds to the structure of PEDOT chain.[42,43] The diffraction peaks of both PEDOT NWs and Te NWs can be observed in the XRD spectrum of the nanocomposite films. When the content of Te NWs content in the composite film is low, the diffraction peaks are not easily observed. As the content of Te NWs increases, the diffraction peaks of Te NWs become more obvious and they are very strong for the nanocomposite with 90 wt% Te NWs.

Fig. 3a shows SEM images of pure PEDOT NWs film. PEDOT NWs in the film formed by vacuum filtration is interwoven together, which may be for this reason that our PEDOT NWs film exhibit high electric conductivity. Fig. 3b and c show SEM images of composite films with different Te NWs contents. Randomly distributed Te NWs can be observed, indicating that Te NWs are well dispersed in PEDOT matrix and form a homogeneous film structure. Clearly, due to the higher electron density of inorganic Te NWs than PEDOT NWs, the Te NWs of the composite films appear bright while the PEDOT NWs matrix appear black or grey in the SEM images. In the Fig. 3d, a higher magnification SEM image clearly shows that Te NWs and PEDOT NWs interweave to form a network microstructure and many polymer/inorganic interfaces.

The room-temperature TE properties of the PEDOT NWs/Te NWs nanocomposite films with different contents of Te NWs are shown in Fig. 4. As observed, pure PEDOT NWs film exhibited power factor of 2.54 μW m^{-1} K^{-2} which is 3 orders of magnitude higher than that of the PEDOT:PSS (0.0027 μW m^{-1} K^{-2}),[26] due to the high σ value of 249.5 S cm^{-1}, and the Seebeck coefficient of 10.08 μV K^{-1} just a slight drop, which may be due to the absence of PSS and the effect of our PEDOT NWs special 1D conductive network structure. As the content of Te NWs increases, the electrical conductivity of the composite films

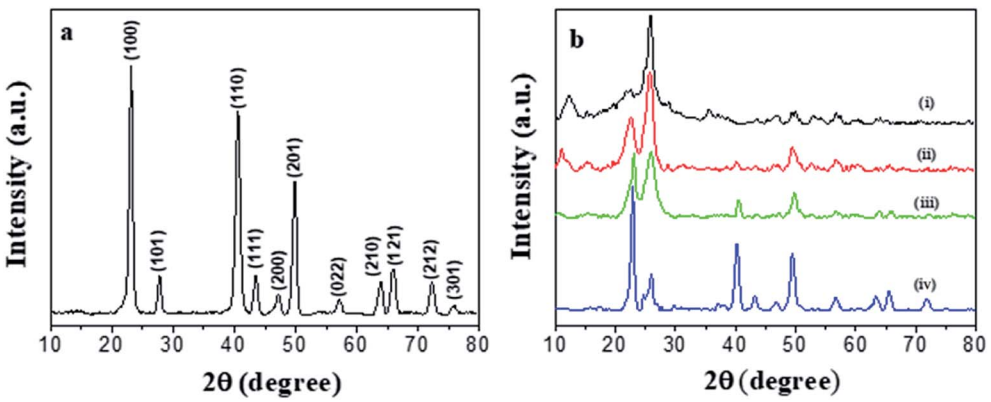

Fig. 2 XRD patterns of Te NWs (a), XRD patterns of different Te NWs contents (b), PEDOT NWs (i), and PEDOT NWs/Te NWs nanocomposite films with 10 wt% (ii), 50 wt% (iii) and 90 wt% (iv) Te NWs.

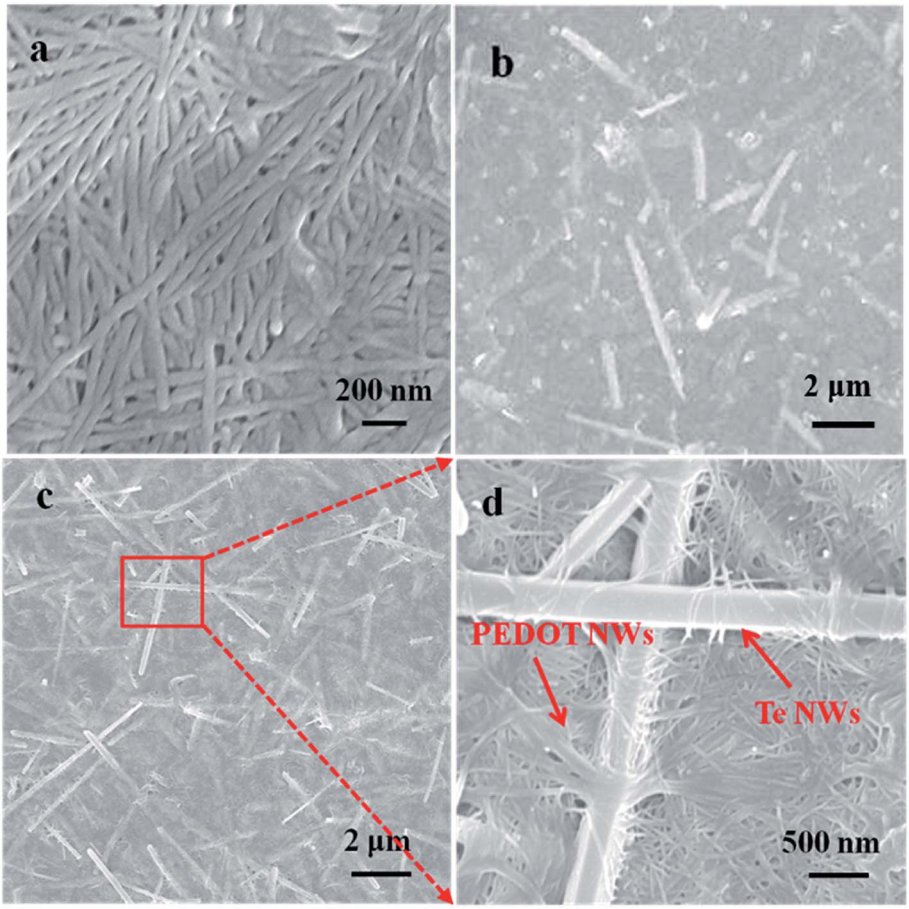

Fig. 3 SEM image of pure PEDOT NWs film (a), PEDOT NWs/Te NWs thin film with 50 wt% Te NWs (b) and 90 wt% Te NWs (c), the high magnification SEM shown in (d) is the red squared portion of the (c).

decreases gradually while the Seebeck coefficient shows an opposite tendency. The enhanced Seebeck coefficient is mainly due to the inherent high Seebeck coefficient of resultant Te NWs (330.04 μV K^{-1}) and "energy filtering" effect[44–47] at the interface between PEDOT NWs and Te NWs. Because in the "energy filtering" process,[48–50] low-energy carriers are scattered by the potential barrier formed by the organic/inorganic interfaces of PEDOT NWs and Te NWs, only high-energy

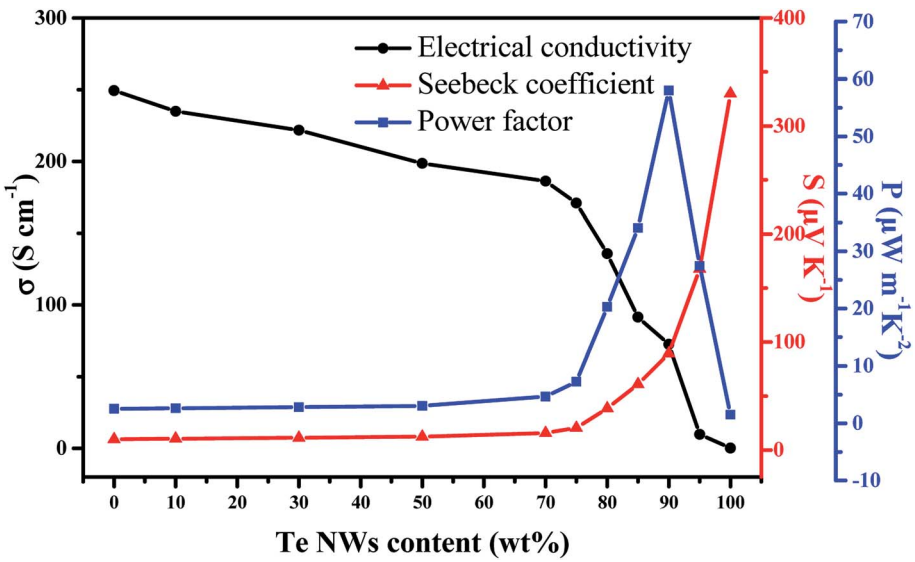

Fig. 4 Thermoelectric properties of PEDOT NWs/Te NWs nanocomposite films with different contents of Te NWs.

Table 1 Comparison between the TE properties at room temperature of reported PEDOT:PSS/Te composites

System	σ (cm^{-1})	S (μV K^{-1})	$S^2\sigma$ (μW m^{-1} K^{-2})	Reference
PEDOT:PSS/Te nanorods treated with H_2SO_4	—	—	42.1	33
PEDOT:PSS/Te nanorod	~700	~27	51.4	41
PEDOT:PSS/Te NWs	—	—	28.5	52
PEDOT:PSS/Te NWs	163(±4)	19.3(±2.3)	70.9	54
PEDOT:PSS/Te NWs doping with EG or DMSO	—	—	100	55
PEDOT:PSS/Te NWs	~150	~0.2	~4.5	56
PEDOT NWs/Te NWs	72.41	89.52	58.03	This work

carriers can pass through the barrier. High-energy carriers can transfer more heat than low-energy carriers, which increase the Seebeck coefficient.[51] Since Te NWs has a relatively low electrical conductivity compared to PEDOT NWs, the electrical conductivity of the nanocomposites decreased with increasing Te NWs content. However, the electric conductivity of the nanocomposite film decreased slowly, especially before Te NWs content was 70 wt%. This is explained by the fact that the conductive link between the PEDOT NWs was not completely broken when the content of PEDOT NWs is low. In addition, many Te NWs–PEDOT NWs–Te NWs junctions are established in PEDOT NWs/Te NWs nanocomposite films. Therefore carriers can also transport through the Te–PEDOT–Te junctions with low energy barrier (in Fig. 3d), so that the decrease of electric conductivity caused by the increase of Te content is hindered.[52] It is worth noting that carrier filtering and other mechanisms of improving the thermoelectric properties are mainly related to the interface and surface area, rather than weight fraction of each component.[53] An optimized power factor (PF = $S^2\sigma$) of 58.03 μV m^{-1} K^{-2} is obtained for PEDOT NWs/Te NWs composites with 90 wt% Te NWs content at room temperature, which is about dozens of times that of the pure PEDOT NWs film and pure Te NWs film. Moreover, the its thermal conductivity was measured and the value of thermal conductivity for the hybrid ranges from 0.423 to 0.502 W (m K)$^{-1}$. Thus, the optimized ZT value is 0.041 at room temperature. All the performance values are comparable with the previous works as showed in Table 1.

Furthermore, it is insightful to consider the temperature dependent thermoelectric properties of the PEDOT NWs/Te NWs (90 wt%) nanocomposite film (as showed in Fig. 5). At a temperature between 100 and 300 K, the Seebeck coefficient of the nanocomposite exhibit p-type semiconductor characteristics and gradually increases strongly with increasing temperature. The electric conductivity shows a negative TCR where the electric conductivity increases with increasing temperature below 300 K. As described by the Mott's variable-range hopping model, the electrical conductivity and Seebeck coefficient would simultaneously increase with increasing temperature,[57] which is consistent with the results we tested. This characteristic is different from the band-like conduction theory in which the Seebeck coefficient and electrical conductivity show anti-correlated with temperature changes.

Fig. 6a shows a prototype of a flexible power generator with PEDOT NWs/Te NWs nanocomposite film as thermoelectric element. Three single-leg of PEDOT NWs/Te NWs (90 wt%) nanocomposite film (length 36 mm, width 6 mm) were adhered to the polyimide tape and the silver wires were used as electrode. The film is fixed to the silver wires with conductive silver paste to ensure good electrical conductivity. One side of the device is in contact with the bubble film. The output performance of the power generator at a temperature difference of 13.5 K is shown in Fig. 6b. The temperature difference is obtained by contacting one end of the device with the wrist and the other end separated from the skin by a bubble film as a thermal insulator. The output voltage of the module is 2.8 mV at a temperature difference of approximately 13.5 K. The output voltage V_0 of the power generator is defined as: $V_0 = NS\Delta T$, where S is the Seebeck coefficient, N is the number of TE elements and the ΔT is temperature difference. For this flexible device, $N = 3$, $S = 89.52$ mV K^{-1}, $\Delta T = 13.5$ K, the V_0 calculated based on these parameters is 3.63 mV, which is higher than the value obtained by the experiment, probably because the actual temperature of the device's hot end is lower than that of the wrist and the inevitable contact resistance in the device. We firstly used PEDOT NWs/Te NWs composite film as raw material to produce flexible wear-resistant thermoelectric devices with high power factors. The preparation process is simple without PSS, which saves cost and reduces environmental pollution.

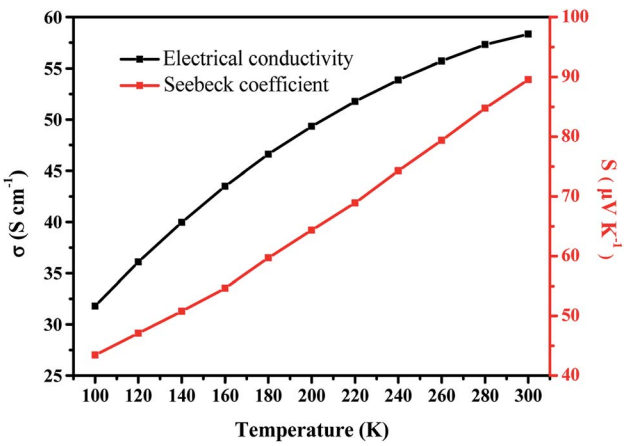

Fig. 5 Temperature-dependent thermoelectric properties of PEDOT NWs/Te NWs (90 wt%) nanocomposite film.

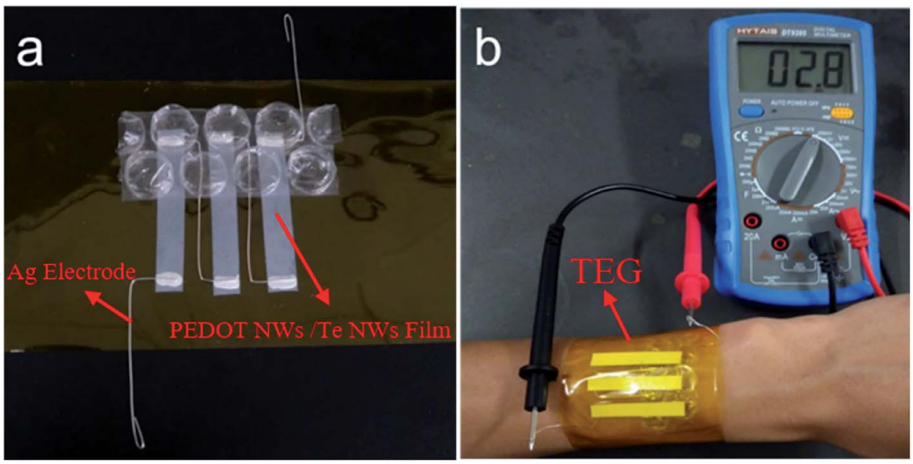

Fig. 6 (a) Photograph of a flexible device prepared using PEDOT NWs/Te NWs (90 wt%) nanocomposite film as a thermoelectric element and (b) output performance of the deviced produced by a temperature difference between wrist (~309.65 K) and the ambient (~296.15 K).

This experimental result provides attempt for the application of flexible TE generators based on PEDOT NWs/Te NWs films in the wearable field.

4. Conclusions

The water soluble PEDOT NWs were synthesized successfully without insulated PSS. Te NWs with high Seebeck coefficient were prepared by solution process. An optimized power factor of 58.03 μW m^{-1} K^{-2} has been obtained for the PEDOT NWs/Te NWs (90 wt%) nanocomposite film. The flexible TE generator exhibits an acceptable output voltage of 2.8 mV at an about 13.5 K temperature difference between environment and human body. It promotes research advances in organic materials in the field of thermoelectric and provides great inspiration for the development of flexible and wearable devices. The obtained films are flexible and are ideal for wearable electronic devices. This study provides a new approach to facilitate practical application of flexible TE generator for low-grade energy harvesting.

Conflicts of interest

There are no conflicts to declare.

Acknowledgements

This study was financially supported by the National Key Research and Development Program of China (Grant no. 2016YFB0303000) and the New Materials Research Key Program of Tianjin (Grant no. 16ZXCLGX00090).

References

1 W. He, G. Zhang, X. Zhang, J. Ji, G. Li and X. Zhao, *Appl. Energy*, 2015, **143**, 1–25.
2 R. J. Stevens, S. J. Weinstein and K. S. Koppula, *Appl. Energy*, 2014, **133**, 80–88.
3 M. K. Kim, M. S. Kim, S. Lee, C. Kim and Y. J. Kim, *Smart Mater. Struct.*, 2014, **23**, 105002.
4 H. Shang, T. Li, D. Luo, L. Yu, Q. Zou, D. Huang, L. Xiao, H. Gu, Z. Ren and F. Ding, *ACS Appl. Mater. Interfaces*, 2020, **12**, 7358–7365.
5 H. Shang, C. Dun, Y. Deng, T. Li, Z. Gao, L. Xiao, H. Gu, D. J. Singh, Z. Ren and F. Ding, *J. Mater. Chem. A*, 2020, **8**, 4552–4561.
6 A. R. M. Siddique, S. Mahmud and B. V. Heyst, *Renewable Sustainable Energy Rev.*, 2017, **73**, 730–744.
7 J. Yuan and R. Zhu, *Appl. Energy*, 2020, **271**, 115250.
8 R. Yue and J. Xu, *Synth. Met.*, 2012, **162**, 912–917.
9 M. Zebarjadi, K. Esfarjani, M. S. Dresselhaus, Z. F. Ren and G. Chen, *Energy Environ. Sci.*, 2012, **5**, 5147–5162.
10 J. Yang, H. L. Yip and A. K. Y. Jen, *Adv. Energy Mater.*, 2013, **3**, 549–565.
11 J. W. G. Bos, H. W. Z. Bergen, M. H. Lee, N. P. Ong and R. J. Cava, *Phys. Rev. B*, 2007, **75**, 195203.
12 J. Dong, W. Liu, H. Li, X. Su, X. Tang and C. Uher, *J. Mater. Chem. A*, 2013, **1**, 12503.
13 W. Shi, L. Zhou, S. Song, J. Yang and H. Zhang, *Adv. Mater.*, 2008, **20**, 1892–1897.
14 Y. Du, S. Z. Shen, K. Cai and P. S. Casey, *Prog. Polym. Sci.*, 2012, **37**, 820–841.
15 Y. Chen, Y. Zhao and Z. Liang, *Energy Environ. Sci.*, 2015, **8**, 401–422.
16 R. Kroon, D. A. Mengistie, D. Kiefer, J. Hynynen, J. D. Ryan, L. Yu and C. Müller, *Chem. Soc. Rev.*, 2016, **45**, 6147–6164.
17 F. Yakuphanoglu, B. F. Şenkal and A. Saraç, *J. Electron. Mater.*, 2008, **37**, 930–934.
18 K. Chatterjee, S. Ganguly, K. Kargupta and D. Banerjee, *Synth. Met.*, 2011, **161**, 275–279.
19 R. Yue and J. Xu, *Synth. Met.*, 2012, **162**, 912–917.
20 Z. Song and H. Zhou, *Energy Environ. Sci.*, 2013, **6**, 2280–2301.
21 O. Bubnova and X. Crispin, *Energy Environ. Sci.*, 2012, **5**, 9345–9362.

22 Q. Yao, L. Chen, W. Zhang, S. Liufu and X. Chen, *ACS Nano*, 2010, **4**, 2445–2451.
23 C. Li, F. Jiang, C. Liu, P. Liu and J. Xu, *Appl. Mater. Today*, 2019, **15**, 543–557.
24 M. Dietrich, J. Heinze, G. Heywang and F. Jonas, *J. Electroanal. Chem.*, 1994, **369**, 87–92.
25 H. Yamato, M. Ohwa and W. Wernet, *J. Electroanal. Chem.*, 1995, **397**, 163–170.
26 J. Kim, R. Patel, B. J. Jung and J. Kwak, *Macromol. Res.*, 2017, **26**, 61–65.
27 W. Lee, Y. H. Kang, J. Y. Lee, K. S. Jang and S. Y. Cho, *RSC Adv.*, 2016, **6**, 53339–53344.
28 Y. Xia and J. Ouyang, *J. Mater. Chem.*, 2011, **21**, 4927–4936.
29 G. H. Kim, L. Shao, K. Zhang and K. P. Pipe, *Nat. Mater.*, 2013, **12**, 719–723.
30 N. Kim, S. Kee, S. H. Lee, B. H. Lee, Y. H. Kahng, Y. R. Jo, B. J. Kim and K. Lee, *Adv. Mater.*, 2014, **26**, 2268–2272.
31 N. Massonnet, A. Carella, G. A. De, J. Faurevincent and J. P. Simonato, *Chem. Sci.*, 2015, **6**, 412–417.
32 J. Liu, X. Wang, D. Li, N. E. Coates, R. A. Segalman and D. G. Cahill, *Macromolecules*, 2015, **48**, 585–591.
33 H. Song, K. Cai and S. Shen, *J. Nanopart. Res.*, 2016, **18**, 386.
34 B. Zhang, J. Sun, H. E. Katz, F. Fang and R. L. Opila, *ACS Appl. Mater. Interfaces*, 2010, **2**, 3170–3178.
35 Y. Wang, K. Cai and X. Yao, *ACS Appl. Mater. Interfaces*, 2011, **3**, 1163–1166.
36 H. Ju and J. Kim, *ACS Nano*, 2016, **10**, 5730–5739.
37 R. A. Horne, *J. Appl. Phys.*, 1959, **30**, 393–397.
38 A. I. Boukai, Y. Bunimovich, J. Tahir-Kheli, J. K. Yu, W. A. Goddard and J. R. Heath, *Nature*, 2008, **451**, 168–171.
39 J. Choi, J. Y. Lee, S. S. Lee, C. R. Park and H. Kim, *Adv. Energy Mater.*, 2016, **6**, 1502181.
40 K. C. See, J. P. Feser, C. E. Chen, A. Majumdar, J. J. Urban and R. A. Segalman, *Nano Lett.*, 2010, **10**, 4664–4667.
41 H. Song and K. Cai, *Energy*, 2017, **125**, 519–525.
42 T. Y. Kim, M. P. Chang, J. E. Kim and K. S. Suh, *Synth. Met.*, 2005, **149**, 169–174.
43 J. W. Choi, M. G. Han, S. Y. Kim, S. G. Oh and S. S. Im, *Synth. Met.*, 2004, **141**, 293–299.
44 D. K. Ko, Y. Kang and C. B. Murray, *Nano Lett.*, 2011, **11**, 2841–2844.
45 M. He, J. Ge, Z. Lin, X. Feng, X. Wang, H. Lu, Y. Yang and F. Qiu, *Energy Environ. Sci.*, 2012, **5**, 8351–8358.
46 K. Zhang, Y. Zhang and S. Wang, *Sci. Rep.*, 2013, **3**, 3448.
47 H. Ju and J. Kim, *ACS Nano*, 2016, **10**, 5730–5739.
48 P. Pichanusakorn and P. Bandaru, *Mater. Sci. Eng., R*, 2010, **67**, 19–63.
49 Y. Zhang, J. H. Bahk, J. Lee, C. S. Birkel, M. L. Snedaker, D. Liu, H. Zeng, M. Moskovits, A. Shakouri and G. D. Stucky, *Adv. Mater.*, 2014, **26**, 2755–2761.
50 C. Gayner and Y. Amouyal, *Adv. Funct. Mater.*, 2019, **30**, 1901789.
51 C. Meng, C. Liu and S. Fan, *Adv. Mater.*, 2010, **22**, 535–539.
52 C. Li, F. Jiang, C. Liu, W. Wang, X. Li, T. Wang and J. Xu, *Chem. Eng. J.*, 2017, **320**, 201–210.
53 J. Xiong, L. Wang, J. Xu, C. Liu, W. Zhou, H. Shi, Q. Jiang and F. Jiang, *J. Mater. Sci.: Mater. Electron.*, 2016, **27**, 1769–1776.
54 K. C. See, J. P. Feser, C. E. Chen, A. Majumdar, J. J. Urban and R. A. Segalman, *Nano Lett.*, 2010, **10**, 4664–4667.
55 S. K. Yee, N. E. Coates, A. Majumdar, J. J. Urban and R. A. Segalman, *Phys. Chem. Chem. Phys.*, 2013, **15**, 4024–4032.
56 S. Ma, K. Anderson, L. Guo, A. Yousuf, E. C. Ellingsworth, C. Vajner, H. T. Wang and G. Szulczewski, *Appl. Phys. Lett.*, 2014, **105**, 073905.
57 Q. Zhang, Y. Sun, F. Jiao, J. Zhang, W. Xu and D. Zhu, *Synth. Met.*, 2012, **162**, 788–793.